A&A 557, A91 (2013)
DOI: 10.1051/0004-6361/201321864

Astronomy & Astrophysics

A multi-epoch spectroscopic study of the BAL quasar APM 08279+5255

I. C IV absorption variability

D. Trevese[1], F. G. Saturni[1], F. Vagnetti[1,2], M. Perna[1], D. Paris[3], and S. Turriziani[2]

[1] Dipartimento di Fisica, Università di Roma La Sapienza, Piazzale Aldo Moro 5, 00185 Roma, Italy
e-mail: dario.trevese@roma1.infn.it
[2] Dipartimento di Fisica, Università di Roma Tor Vergata, via della Ricerca Scientifica 1, 00133 Roma, Italy
[3] Osservatorio Astronomico di Roma, via Frascati 33, 00040 Monte Porzio Catone, Italy

Received 9 May 2013 / Accepted 15 July 2013

ABSTRACT

Context. Broad absorption lines indicate gas outflows with velocities from thousands of km s^{-1} to about 0.2 the speed of light, which may be present in all quasars and may play a major role in the evolution of the host galaxy. The variability of absorption patterns can provide information on changes in the density and velocity distributions of the absorbing gas and its ionisation status.
Aims. We want to accurately follow the evolution in time of the luminosity and both the broad and narrow C IV absorption features of an individual object, the quasar APM 08279+5255, and analyse the correlations among these quantities.
Methods. We have collected 23 photometrical and spectro-photometrical observations at the 1.82 m Telescope of the Asiago Observatory since 2003, plus 5 other spectra from the literature. We analysed the evolution in time of the equivalent width of the broad absorption feature and two narrow absorption systems, the correlation among them and with the *R* band magnitude. We performed a structure function analysis of the equivalent width variations.
Results. We present an unprecedented monitoring of a broad absorption line quasar based on 28 epochs during 14 years. The shape of broad absorption feature shows relative stability, while its equivalent width slowly declines until it sharply increases during 2011. At the same time, the *R* magnitude stays almost constant until it sharply increases during 2011. The equivalent width of the narrow absorption redwards of the systemic redshift only shows a decline.
Conclusions. The broad absorption behaviour suggests changes in the ionisation status as the main cause of variability. We show for the first time a correlation of this variability with the *R* band flux. The different behaviour of the narrow absorption system might be due to recombination time delay. The structure function of the absorption variability has a slope comparable with typical optical variability of quasars. This is consistent with variations of the 200 Å ionising flux originating in the inner part of the accretion disk.

Key words. galaxies: active – quasars: absorption lines – quasars: general – quasars: individual: APM 08279+5255

1. Introduction

The broad absorption line (BAL) quasars (QSOs) were discovered by Lynds (1967), and their properties are described in Weymann & Foltz (1983), Turnshek (1988). The spectra of about 20% of all QSOs exhibit BALs with velocities from thousands of km s^{-1} to $\lesssim$0.2 the speed of light, indicating the outflow of material and energy from the active galactic nucleus (AGN) to the surrounding space (Hewett & Foltz 2003; Gibson et al. 2008; Capellupo et al. 2011). Mechanical and radiative energy transfer to the QSO environment can affect the galaxy evolution processes, so that understanding gas outflows has become crucial in establishing the role played by the AGN feedback in the cosmological process of galaxy formation and evolution (Cattaneo et al. 2009, and references therein), as suggested, in particular, in the case of the "ultra-fast outflows" detected in X-rays in several $z < 0.1$ AGNs (Tombesi et al. 2010) and specifically in APM 08279+5255 (Chartas et al. 2009), which is the subject of the present study.

That BALs only appear in a fraction of QSO spectra, may indicate that either they are only seen in particular directions with respect to the axis of the accretion disk (Elvis 2000, and references therein) or they are observed during particular phases of the QSO life (Farrah et al. 2007, and references therein). Investigating the nature and location of these outflowing absorbers could, in principle, provide clues to understanding the dynamics and ionisation processes in the circumnuclear gas. Unfortunately, structure, location, dynamics, and ionisation state of the absorbers are poorly known so far. The variability of BALs can provide other important information about the properties of the absorbing gas. BAL variations were first detected by Foltz et al. (1987) (see also Barlow et al. 1992, and references therein). Variability may be caused by the motion of gas clouds across the line of sight, or by changes in the ionisation status of the gas.

A first systematic analysis of BAL variability was presented by Barlow (1993), who analysed 23 BALQSOs, each observed typically two to three times in the course of four years. Continuum variations were only associated with BAL variation in some cases, suggesting the possibility that changes in the ionisation status could cause absorption variability, possibly with some phase difference between the far UV ionising flux and the observed continuum changes. Since then, some other systematic studies have been devoted to analysing BAL variability. They mainly focus on C IV BAL, which is usually the most visible absorption feature.

Lundgren et al. (2007) used the Sloan Digital Sky Survey (SDSS; York et al. 2000) spectra of 29 BAL QSOs, observed twice in a total observing period of about one year, corresponding to rest-frame time lags in the range of two weeks to four months. Their analysis is limited to those BALs that are separated from the emission peak by more than 3600 km s^{-1}, to avoid the complication from the emission line variability. They observe that the strongest BAL variability occurs among absorption features with the smallest equivalent widths and with velocities exceeding 12 000 km s^{-1}. They conclude that strong variability at high velocity might be consistent with Kelvin-Helmholtz instabilities predicted in disk-wind models of Proga et al. (2000).

Gibson et al. (2008) studied the BAL variations on long timescales of 13 QSOs, in the redshift range 1.7−2.8, taking advantage of the overlap between the Large Bright Quasar Survey (LBQS; Hewett et al. 1995, and references therein) and SDSS, which observed these objects with time differences of 10 to 18 years, corresponding to rest-frame time lags in the range of 3 to 6 years. They find that the equivalent width variations tend to increase with the time lag, in the observed interval. They find no evidence that variations are dominated by changes in the photo-ionisation on multi-year timescales. A subsequent study by Gibson et al. (2010) analysed the variations of nine BALQSOs in two to four epochs, considering both C IV and Si IV BALs. They find some correlation between C IV and Si IV equivalent width variations, estimate lifetimes $\gtrsim$30 yr for the stronger BALs, and do not find asymmetries in the growth and decay timescales.

Capellupo et al. (2011) report the first results of new observations of the Barlow (1993) sample, obtained with the 2.4 m Hiltner telescope of the MDM Observatory, supplemented with SDSS spectra, for a total of 120 spectra for 24 objects. This study provides a comparison among short and long time scale variations and indicates a dependence of variability on the velocity of the outflow and the BAL strength. A subsequent study by Capellupo et al. (2012), presents further results on their monitoring of 24 BALQSOs and compares C IV and Si IV BAL variability, suggesting a complex scenario that seems to favour ionisation changes of the outflowing gas, while at the same time variations in limited portions of the broad absorption troughs may indicate movements of the individual clouds across the line of sight. A further contribution by Capellupo et al. (2013) is focussed on the short time-scale variability of the C IV BAL from the same sample. Variations in only portions of the BAL suggest the presence of substructures in the outflow, moving across the line of sight, and provide constrains on the speed and geometry of the outflows.

Clearly, the amount of data, both in terms of number of different objects and sampling frequency of the individual quasars, is crucial to assessing the properties of BAL variability. Sampling of individual QSOs is, however, limited by the intrinsic timescales of variations, especially for high-redshift objects. In the present study, we discuss the result of the monitoring of a single object, APM 08279+5255 at $z = 3.911$, which we have observed 23 times since 2003 in the framework of a monitoring campaign of medium-high-redshift QSOs, carried out with the 1.82 m Copernico telescope of the Asiago Observatory and devoted to determining the mass of the central supermassive black hole (SMBH) through reverberation mapping (Trevese et al. 2007). Since APM 08279+5255 is one of the brightest QSOs in the sky and shows several other interesting peculiarities, it was observed several times by other authors, photometrically and spectroscopically, soon after its discovery (Irwin et al. 1998), so that it was possible to collect both spectroscopic and photometric data from the literature, which have been included in the present analysis, providing what is, to our knowledge, the best sampling of the variability of a BAL QSO available to date. In Sect. 2 we describe the data we collected from the literature, in Sect. 3 we describe our spectrophotometric monitoring campaign and data reduction, in Sect. 4 we analyse the variability of the C IV absorption systems and its correlation with photometric variability, and in Sect. 5 we discuss and summarise the results.

2. Data from the literature

2.1. Spectroscopy

The BAL QSO APM 08279+5255 was serendipitously discovered in the course of a survey conducted with the 2.5 m *Isaac Newton* Telescope (INT), La Palma, for the identification of cool carbon stars in the Galactic halo (Irwin et al. 1998). Observations were taken between February 27 and March 6, 1998 with a resolution $\lambda/\Delta\lambda \sim 2000$, and a redshift $z = 3.87$ was initially attributed on the basis of the Si IV + O IV] feature, the C III] λ1909 Å at ~9300 Å, and Nv λ1240 at 6040 Å. M.J. Irwin kindly provided us with the data of the discovery spectrum, which are included in the present analysis. This object, with a magnitude $R = 15.2$, appeared as the brightest QSO in the sky, with a bolometric luminosity exceeding $\sim 5 \times 10^{15} L_{\odot}$, and it has been the subject of a great number of papers, of which we mention only those that are relevant to the specific purpose of our study.

Thanks to its high redshift, APM 08279+5255 is an ideal "background" source for analysing the intervening absorptions. In fact, high-resolution ($R \approx 50\,000$) spectra were taken with the HIRES spectrograph at the Keck telescope for analysing the Lyα clouds distribution and metal abundances (Ellison et al. 1999, 2004). A low-resolution spectrum ($\lambda/\Delta\lambda \sim 400$) was obtained by Hines et al. (1999), together with polarised spectra that permitted identification of a broad O VI $\lambda\lambda$1032, 1038 Å absorption, associated with Lyβ, falling in the Lyα forest. Also this spectrum, kindly provided by D.C. Hines, is included in the present analysis. Soon after the discovery, adaptive optics images at CFHT telescope have shown APM 08279+5255 to be a double source, likely gravitationally lensed (Ledoux et al. 1998), as already proposed by Irwin et al. (1998). *Hubble* Space Telescope (HST) and radio images have suggested that there is a long-sought "third component", which is expected in the case of axi-symmetric gravitational lensing fields (Ibata et al. 1999). A lens model indicating a magnification of about 100 was derived by Egami et al. (2000). Spectroscopic HST observations, at medium-high-resolution ($\lambda/\Delta\lambda \sim 4500$) confirmed that the third component is in fact part of the lensed image (Lewis et al. 2002). Besides providing two more epochs for the spectroscopic monitoring, Keck and HST spectra are also used in our analysis to resolve and identify absorption features that are not resolved in our spectra.

The HST spectrum was obtained by Lewis et al. (2002) with STIS. High-resolution spectra allowed us to identify the absorption-free regions, shown in Fig. 1, that can be used to fit the C IV emission line profile. The same figure also shows two narrow absorption line (NAL) systems: the first, identified by Ellison et al. (2004), which we call "red-NAL", falls on the red wing of the C IV emission, is close to the systemic redshift, and is partly overlapped by the Fraunhofer A band of O_2. The second, which we call "blue-NAL", is overlapped by

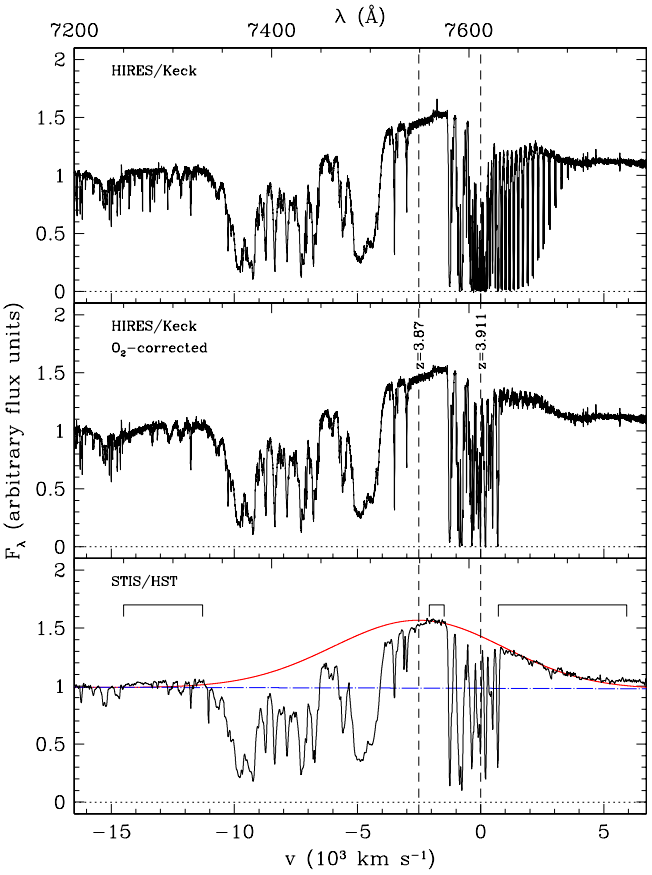

Fig. 1. The (uncalibrated) flux in the $\lambda\lambda$7200–7780 Å region. *Top panel*: from the Keck HIRES high-resolution spectrum (Ellison et al. 1999); *middle panel*: the same spectrum after correction for telluric O_2 band (see Sect. 3); *bottom panel*: from HST STIS spectrum (Lewis et al. 2002), where the continuum (blue dashed line) and a Gaussian fit to the C IV emission line (red curve) are shown. A comparison of middle and bottom panels shows that the O_2 correction is satisfactory. The velocity scale is based on the systemic redshift $z = 3.911$ (Downes et al. 1999).

the BAL and is discussed in Srianand & Petitjean (2000). A continuum, extrapolated from two absorption-free regions bluewards of C IV emission (see Sect. 4), is also shown. A Gaussian fit to the emission line provides a width $\sigma_{\rm CIV} = 3450\pm60$ km s^{-1}.

Another spectrum of resolution $\lambda/\Delta\lambda \sim 700$, obtained at the Telescopio Nazionale *Galileo* (TNG), La Palma, in 2011 (Piconcelli et al., in prep.) has also been included in the analysis.

2.2. Photometry

Photometry in the R band of APM 08279+5255 was obtained by Lewis et al. (1999) for 23 epochs between April 1998 and June 1999, with the main goal of studying the intrinsic or microlensing character of variability. They provided relative magnitudes with respect to a reference star S_2, for the QSO and three other stars in the field, S_1, S_3, S_4 (see their Fig. 1), for the purpose of choosing the best reference star.

We also measured R band magnitude difference with respect to another star S, which we adopt as a reference for spectrophotometric measurements (see Sect. 3). Unfortunately, this star is not included in the Lewis et al. (1999) field. However, their star S_1 is included in our field, so that we can rescale their photometry to ours, by defining

$$\Delta R_{QS} = R_Q - R_2 + \langle R_2 - R_1\rangle + \langle R_1 - R_S\rangle \quad (1)$$
$$\Delta R_{1S} = R_1 - R_2 + \langle R_2 - R_1\rangle + \langle R_1 - R_S\rangle$$

where $\langle R_2 - R_1\rangle$ and $\langle R_1 - R_S\rangle$ are average values computed on the Lewis et al. (1999) and our light curves, respectively.

Despite the larger uncertainty of R_1 compared to those of R_2 or R_S, the uncertainty on the inter-calibration of the two data sets given by the average quantity $b = \langle R_2 - R_1\rangle + \langle R_1 - R_S\rangle$ is $\sigma_b = [\sigma^2_{2-1}/(N_{2-1}-1)+\sigma^2_{1-S}/(N_{1-S}-1)]^{1/2} \sim 0.005$ mag, where $N_{1-2} = 23$ and $N_{1-S} = 24$ indicate the number of observations in the Lewis et al. (1999) and our monitoring campaigns, respectively. This quantity is smaller than the internal uncertainties of the individual data sets $\sigma_{1-2} \sim 0.023$ mag and $\sigma_{1-S} \sim 0.009$. The latter, in turn, can be assumed as conservative estimates of the uncertainty on the QSO photometry. In total we have at our disposal 49 photometric observations from 1998 to 2012 that can be correlated with spectral variations. The complete light curve is shown in Fig. 6.

3. Observations and data reduction

In 2003 we started a spectrophotometric monitoring campaign aimed at measuring the mass of four luminous QSOs (Trevese et al. 2007) by the reverberation mapping technique (Blandford & McKee 1982; Peterson 1993). Observations were carried out at the 1.82 m Copernicus telescope of the Asiago Observatory, equipped with the Faint Object Spectrograph & Camera (AFOSC). Spectroscopic observations were carried out using a 8.″44-wide slit and a grism with a dispersion of 4.99 Å pixel^{-1}, providing a typical resolution of ~15 Å in the spectral range 3500–8500 Å ($\lambda/\Delta\lambda \sim 400$). Exposures were carried out after orienting the slit to include both the QSO and a reference star S of comparable magnitude ($R = 14.4$), located at α 08 31 22.3 δ +52 44 58.6 (J2000), as internal spectrophotometric calibrator. The wide slit avoids both differential diffraction effects and possible different fractional losses of the QSO and the reference star, but limits the accuracy of the wavelength scale. In fact, the position of the QSO can fluctuate within the slit, affecting both the line profile and the position on the wavelength scale. Thus, after the calibration with the spectral lamps, the λ scale must be readjusted, and the entire procedure has a residual uncertainty of ~3 Å rms.

Typical spectroscopic observations consisted of two subsequent exposure of 1800 s each, plus direct images in the R band to detect possible variations of the reference star with respect to other stars in the ~8 × 8 arcmin^2 field centred on the QSO. A journal of the observations is given in Table 1, where the INT, Keck, Steward, HST, and TNG observations are also indicated. In total we have 28 spectra from 1998 to 2012.

The data reduction is described in Trevese et al. (2007) and briefly summarised below. The spectra $Q(\lambda)$ of the QSO and $S(\lambda)$ of the reference star were extracted with the standard IRAF procedures. The QSO/star ratio is computed for each exposure $k = 1, 2$:

$$\mu^{(k)}(\lambda) = Q^{(k)}(\lambda)/S^{(k)}(\lambda). \quad (2)$$

This quantity is independent of extinction changes during the night. This allowed us to check for consistency between the two exposures and to reject the data if inconsistencies occurred (under the assumption that intrinsic QSO variations are negligible

Table 1. List of the observations.

Date	MJD	Telescope
1998 Mar.	50 875.7	INT[b]
1998 May	50 945.8[a]	Keck[c]
1998 Nov.	51 132.5	Steward Obs.[d]
2001 Dec.	52 270.4[a]	HST[e]
2003 Feb.	52 695.4	Asiago Obs.
2003 Nov.	52 963.6	″
2004 Feb.	53 047.3	″
2004 Feb.	53 049.3	″
2005 Jan.	53 388.4	″
2005 Apr.	53 475.3	″
2006 Mar.	53 797.5	″
2006 Nov.	54 068.7	″
2006 Dec.	54 091.4	″
2007 Feb.	54 145.3	″
2007 Apr.	54 201.3	″
2007 Dec.	54 435.7	″
2008 Jan.	54 472.5	″
2008 Feb.	54 513.4	″
2008 Dec.	54 807.6	″
2009 Jan.	54 835.4	″
2009 Feb.	54 884.3	″
2009 Mar.	54 914.4	″
2011 Apr.	55 653.3	″
2011 May	55 684.4	TNG[f]
2011 Nov.	55 894.5	Asiago Obs.
2011 Dec.	55 915.5	″
2012 Feb.	55 985.3	″
2012 Nov.	56 238.4	″

Notes. [(a)] Average of the observing MJD, [(b)] Irwin et al. (1998), [(c)] Ellison et al. (1999), [(d)] Hines et al. (1999), [(e)] Lewis et al. (2002), [(f)] Piconcelli et al. (in prep.) .

during 1 h of observing time). In fact, typical spectra of two consecutive exposures have a ratio $\mu^{(1)}(\lambda)/\mu^{(2)}(\lambda)$ of order unity, with deviations smaller than 0.02 when averaged over 500 Å, at least in the 4000 Å−7000 Å range. When discrepancies were greater than 0.04, both the exposures were rejected. A registration of the wavelength scale among different exposures was necessary owing to small changes of the object position within the wide slit (which are in general negligible in the case of pairs of consecutive exposures). Then, the QSO and star spectra taken in the two exposures were co-added and the ratio

$$\mu_i(\lambda) = \left(Q_i^{(1)} + Q_i^{(2)}\right) / \left(S_i^{(1)} + S_i^{(2)}\right) \quad (3)$$

computed, at each epoch i.

The reference star was flux-calibrated at a reference epoch, and the main telluric absorption features (Fraunhofer A and B bands $\lambda\lambda 7594, 6867$ Å and water $\lambda 7245$ Å) were removed from the calibrated spectrum by interpolating the relevant absorption region with a spline function through the spectral points in two intervals around each absorption feature. This provides us with a flux-calibrated absorption-free spectrum of the reference star $f^S(\lambda)$. All the flux-calibrated quasar spectra were then obtained as $f_i^Q(\lambda) \equiv \mu_i(\lambda) f^S(\lambda)$. The calibrated star spectrum $f^S(\lambda)$ adopted is the same for all epochs, thus it does not affect the *relative* flux changes.

We also stress that the telluric absorption features were removed in this way since they do not affect the value of $\mu_i(\lambda)$. The same is obviously true for the differences in airmass and atmospheric extinction. This is true, in particular, for the Fraunhofer

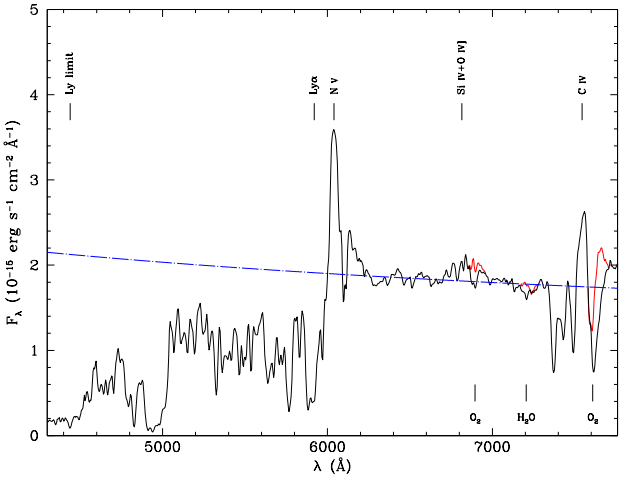

Fig. 2. Spectrum of APM 08279+5255 obtained with the AFOSC camera at the 1.82 m Copernicus Telescope of the Asiago Observatory. The identification of the main absorption and emission features are indicated. The red line represents the correction for the telluric O_2 and H_2O bands. A power-law fit through spectral regions relatively free of absorption or emission features is also shown (see Sect. 4.1).

A band that, in the case of APM 08279+5255, falls just redwards of the C IV emission line and is also partially overlapped by the already mentioned C IV "red-NAL" at $z \sim 3.911$. An example of calibrated spectrum obtained at the Copernico telescope is shown in Fig. 2. Thanks to the availability of the high-resolution spectrum obtained at Keck telescope by Ellison et al. (1999), we checked that the procedure adopted to remove the telluric absorptions in low-resolution spectra was satisfactory, at least to a first order. This was checked by first correcting for O_2 absorption the high-resolution spectrum, where the individual lines of the band were detected, using the spectrum of the calibration star (Feige 34). Then we smoothed the corrected spectrum, down to the resolution $\lambda/\Delta\lambda \sim 400$ of our spectra. For comparison, we smoothed down both the QSO and calibration star spectra to the same resolution, without correcting for O_2 absorption. We then applied the procedure adopted on our low-resolution data to remove telluric absorptions. The equivalent width of the C IV absorption feature, computed in both cases, appears consistent within 5%, even though the Keck spectra of the QSO and the calibration star were not taken simultaneously, as is instead the case for our QSO and the reference star S.

4. Spectral variability

4.1. The BAL and NAL equivalent width variability

The present analysis is focussed on the spectral region around C IV emission, whose evolution in time is shown in Fig. 3. We stress that at the time of discovery, the systemic redshift was assumed $z = 3.87$ and was later revised to $z = 3.911$, as measured by Downes et al. (1999) from CO(4−3) and CO(9−8) molecular lines at $\lambda 650\ \mu$m and $\lambda 290\ \mu$m, implying a Doppler blueshift velocity of 2500 km s^{-1} for the emission lines. While Lundgren et al. (2007) include in their sample only BALs that are separated from the associated emission peak by more than 3600 km s^{-1}, we are in contrast forced to consider the absorption occurring on the blue wing of the emission line, since in our case the BAL is separated from the peak by less than 800 km s^{-1}. At each epoch, we compute a continuum as a power-law fit through the observed spectrum, in two wavelength intervals that are free of

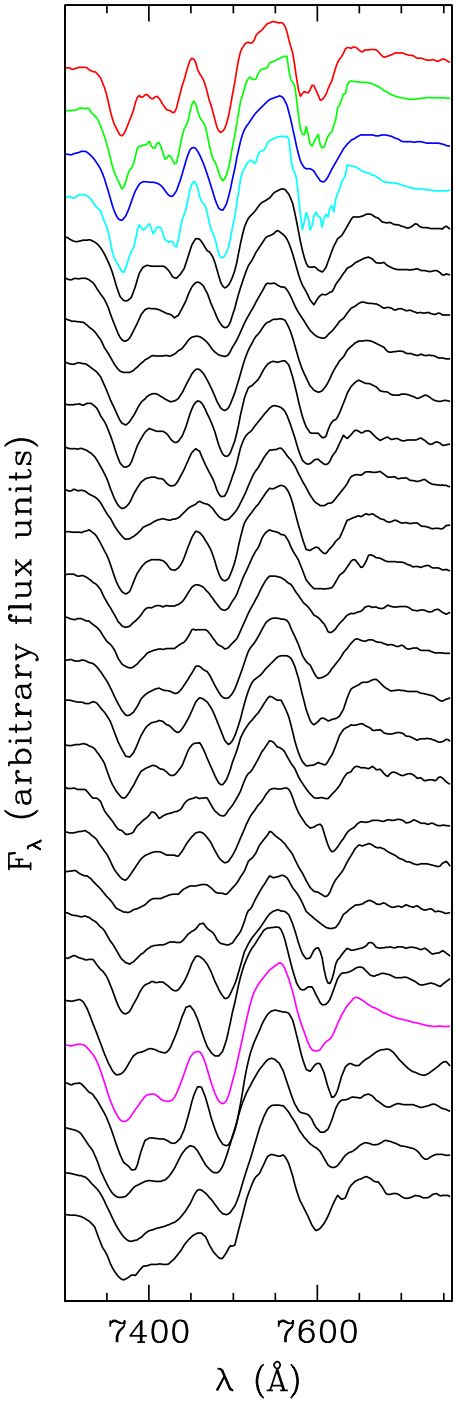

Fig. 3. Evolution in time of the spectral region around C IV emission line. From top to bottom, the first (red) and third (blue) spectra correspond to INT and Steward Observatory data, the second (green), the fourth (cyan), and 24th (magenta) epochs correspond respectively to Keck, HST, and TNG spectra, smoothed to match the resolution of the Asiago spectra (see Table 1). All spectra are shown with the same flux scale and an arbitrary shift between each other. At a glance it is clear that the BAL feature retains its global *shape* with time.

major emission or absorption features. The rest-frame regions $\lambda\lambda$1250−1370 Å and $\lambda\lambda$1440−1470 Å were selected following Capellupo et al. (2011) and Barlow et al. (1992), respectively, for consistency (but see also Vanden Berk et al. 2001). The C IV emission line profile is strongly affected by the BAL, on the blue side, and by the Fraunhofer A band plus the red-NAL system on the red side. However, we can use both the Keck and HST spectra to identify the unabsorbed wavelength intervals around C IV and fit the emission line profile.

We fit the emission line with a Gaussian profile, keeping the central wavelength fixed to the value corresponding to $z = 3.87$, which was deduced from the Si IV+O IV], C III], and N V (Irwin et al. 1998), and the line width to the value $\sigma_{\rm CIV} = 3450 \pm 60$ km s^{-1} (see Sect. 2), while letting the line amplitude be the sole varying parameter. In doing this, we are assuming that relative amplitude changes are larger than the relative changes in the shape of the line. We can now consider a pseudo-continuum consisting in a proper combination of continuum and emission line fluxes. The spatial location and the size of the absorbing gas is unknown, and it could cover only part of the continuum and/or emission line sources. Thus we can write the observed flux as

$$f(\lambda) = f_{\rm c}(1-\xi_{\rm c}) + f_{\rm l}(1-\xi_{\rm l}) + (\xi_{\rm c} f_{\rm c} + \xi_{\rm l} f_{\rm l}) {\rm e}^{-\tau(\lambda)} \quad (4)$$

where $f_{\rm c}, \xi_{\rm c}, f_{\rm l}, \xi_{\rm l}$ indicate the continuum and emission line fluxes and covering factors, and $\tau(\lambda)$ is the optical depth, which in a simple model is assumed to be the same for photons emitted from the continuum source and the emitting clouds. Since the size of the continuum-emitting region is expected to be much smaller than the broad line region (BLR) size, then $\xi_{\rm l} \le \xi_{\rm c}$. In the following we assume $\xi_{\rm c} = 1$. Moreover, the high-resolution Keck spectrum shows that some individual absorption features in the BAL have a residual flux that is smaller than the emission line flux at the same wavelength (see Fig. 1), implying that the pseudo-continuum, which is absorbed by the outflowing gas, must contain a contribution from the emission line corresponding to $\xi_{\rm l} \ge (1 - f/f_{\rm l}) \approx 0.3$. Thus we compute the equivalent widths W:

$$W(t) = \int \frac{f_{\rm c} + f_{\rm l} - f}{\xi_{\rm c} f_{\rm c} + \xi_{\rm l} f_{\rm l}} {\rm d}\lambda \quad (5)$$

according to the two extreme assumptions $\xi_{\rm l} = 1$ and $\xi_{\rm l} = 0.3$, the former corresponding to the pseudo-continuum adopted by Capellupo et al. (2011). The values of $W(t)$ computed with $\xi_{\rm l} = 0.3$ are a factor ≈1.2 higher than for $\xi_{\rm l} = 1$. This factor, however, is virtually constant in time and thus does not affect the following discussion of the time behaviour of the absorption. We therefore adopt $\xi_{\rm l} = 1$ from here on.

The uncertainty on the equivalent width W_i at the ith epoch is estimated as follows. Since in our monitoring we have two exposures of 1800 s for each spectrum, we compute the difference $\delta W_i = |W_i^{(2)} - W_i^{(1)}|$ between the equivalent width as computed with each exposure. They appear correlated with the equivalent widths W_i. Thus we assume constant fractional uncertainty $\varepsilon = (\langle(\delta W/W)^2\rangle)^{\frac{1}{2}}$, where the angular brackets indicate the average on the entire set of measurements, and we adopt $\sigma_W = \varepsilon W$ as rms error, where $\varepsilon = 0.06$. From Fig. 3 it appears that the general shape of the absorbing systems is conserved in time, as stated quantitatively in the following. High-resolution spectra show that the absorption bluewards of C IV emission consists of two main broad structures around −10 000 and −4500 km s^{-1}, respectively (see Fig. 1), and the system of narrow absorption lines, between −9000 and −7000 km s^{-1} (Srianand & Petitjean 2000), which we call "blue-NAL". In our low-resolution spectra (see Fig. 4) we decompose the absorption profile by fitting two Gaussians in the spectral regions $\lambda\lambda$7300−7390 Å and $\lambda\lambda$7470−7510 Å, respectively, corresponding to the two broad structures (see Fig. 1). A third structure, corresponding to the "blue-NAL", is obtained as the residual spectrum after the two

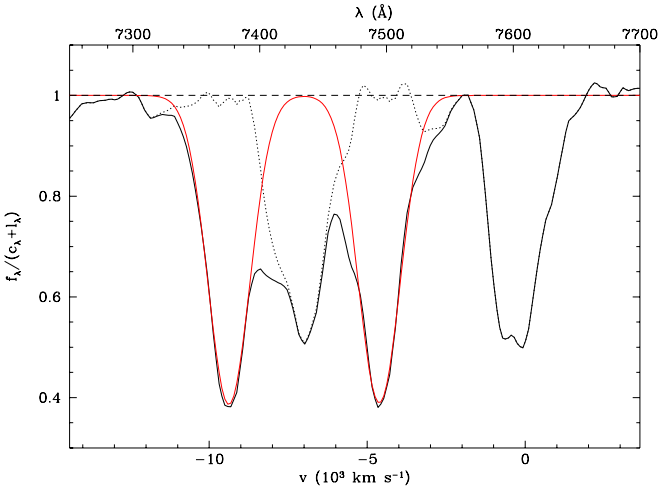

Fig. 4. Decomposition of the C IV absorption structure at a particular epoch (MJD 52 695.4). The flux is divided by the pseudo-continuum computed with $\xi_c = \xi_l = 1$. Two Gaussian profiles (red) represent the main component BAL_1 and BAL_2 of the BAL. The dotted line is the residual absorption corresponding to the blue NAL. The velocity scale is based on the systemic redshift $z = 3.911$.

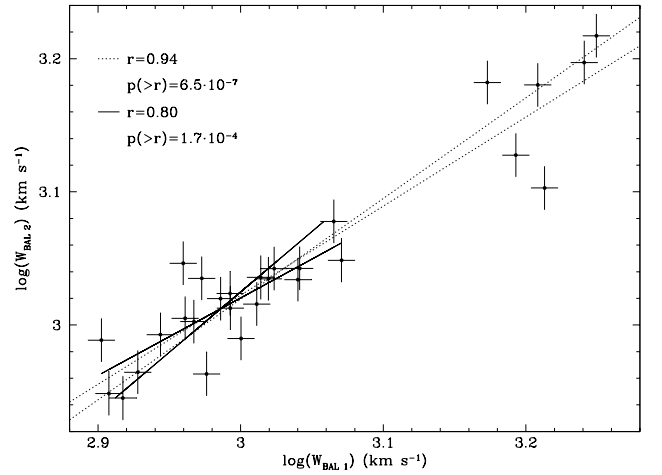

Fig. 5. Logarithms of the equivalent widths W_{BAL_1} and W_{BAL_2} expressed in km s^{-1}. The continuous and dotted pairs of regression lines (one component versus the other and vice versa) are computed by respectively excluding or including the observations at the last 6 epochs. The correlation coefficients and the relevant probabilities of the null hypothesis are indicated. The correlation is high and statistically significant also when the last 6 points are excluded.

Gaussian components are subtracted. The Gaussians have no physical meaning, but they are simply used to describe apparent structures at the resolution of our spectra. Of course, the "blue-NAL" residual might be affected by an unknown contribution from the broad absorption.

The central wavelengths λ_1 and λ_2, the widths σ_1 and σ_2 and the amplitudes of both the Gaussian components are free parameters in the fit performed at each epoch. The average central wavelengths of the two BAL features are $\bar{\lambda}_1 = 7373$ Å and $\bar{\lambda}_2 = 7489$ Å, and the relevant standard deviations are $\Sigma_{\lambda_1} = \Sigma_{\lambda_2} = 3$ Å. The central wavelengths of the BAL components show small random shifts, comparable to the uncertainty of our wavelength scale. Instead, the amplitudes of both the components undergo significant changes. However the variations in

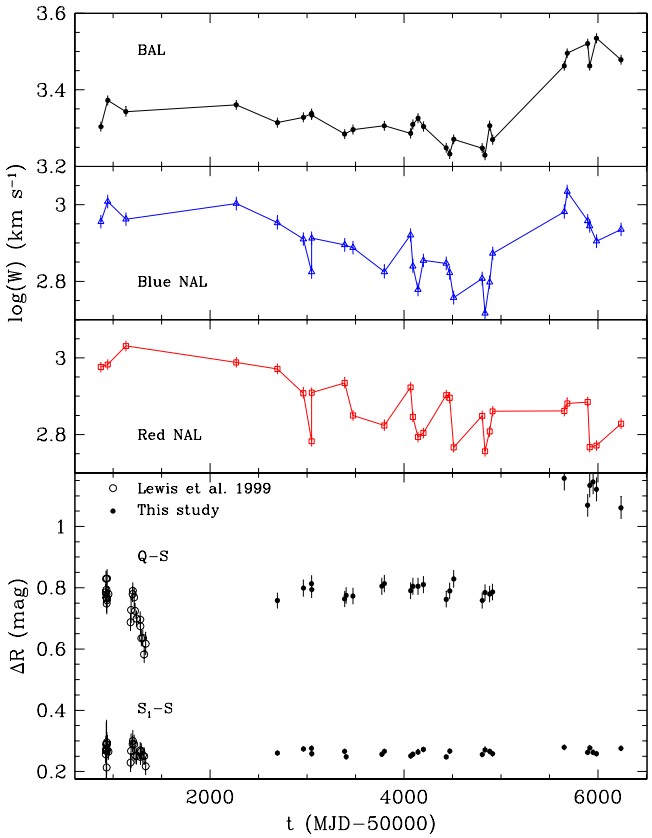

Fig. 6. *Upper panels*: equivalent widths W_{BAL}, W_{NALb}, and W_{NALr} of the C IV absorptions as a function of time. *Bottom panel*: R band light curve ΔR_{QS} of APM 08279+5255 normalised to the reference star S adopted in the Asiago monitoring campaign (upper curve). For comparison, the magnitude difference ΔR_{1S} between the star S_1 and our reference star S is also reported as an indication of the photometric accuracy. Photometry, relative to the star S, is computed from magnitude differences in our data, while it is recalculated according to Eq. (1) for Lewis et al. (1999) data.

their equivalent widths W_{BAL_1} and W_{BAL_2} are strongly correlated, $r_{1,2} = 0.94$, $P(>r_{1,2}) = 6.5 \times 10^{-7}$, as shown in Fig. 5 where the equivalent widths are computed in units of velocity with respect to the emission line, for consistency with the literature. This suggests considering $W_{BAL} = W_{BAL_1} + W_{BAL_2}$ as representative of the total BAL absorption, in the subsequent variability analysis. This behaviour is completely different from that of FBQS J1408+3054, which exhibits strong changes in the absorption shape, suggesting that the motion of part of the absorbing clouds is out of the line of sight (Hall et al. 2011). For the red and blue NAL systems, we compute the relevant equivalent widths W_{NALr} and W_{NALb} by simply integrating the residuals in the ranges 7550–7660 Å and 7380–7480 Å. Figure 6 shows W_{BAL}, W_{NALr}, and W_{NALb} as functions of time t = MJD − 50 000. All of these quantities show a slow decreasing trend from $t \sim 1000$ to $t \sim 5000$. Subsequently, the W_{BAL} undergoes a sudden increase, while W_{NALr} continues the downwards trend. W_{NALb} shows an intermediate behaviour, but it might be affected by the BAL absorption. High-resolution monitoring is needed to disentangle BAL and NAL absorption variations in this spectral region.

The overall appearance of the BAL structure is relatively stable (two minima, with no significant wavelength variation, and amplitudes varying proportionally), while its equivalent width

changes significantly. This suggests that the global properties of the density and velocity fields of the absorbing gas remain unchanged during variations in $W(t)$. The simplest explanation of such behaviour is a change in the ionisation status of the absorbing gas. This conclusion is independent of the correlation of $W(t)$ with the variations in the R band continuum, which is discussed in the next section. In fact, the R band measures the continuum at $\lambda \approx 1300$ Å, while the ionising continuum, relative to the $C^{3+} \rightarrow C^{4+}$ transition, corresponds to $\lambda_{3,4} \approx 200$ Å, and the two continua are not necessarily correlated. However, the shape of the BAL structure is not strictly constant, since the average slope in Fig. 5 is about 0.7, implying a decrease in the ratio $W_{\mathrm{BAL}_2}/W_{\mathrm{BAL}_1}$ for increasing W_{BAL}. This is discussed in Sect. 5.

4.2. Correlation analysis

So far, we have not considered the relation between the absorptions changes and the source brightness variations ΔR of the R magnitude. For the four quantities W_{BAL}, $W_{\mathrm{NAL}r}$, $W_{\mathrm{NAL}b}$, and ΔR, we can analyse six scatter plots (Fig. 7), the relevant correlation coefficients, and probabilities of the null hypothesis. We comment on each in turn.

a) W_{BAL} vs. ΔR. These quantities show a strong and significant correlation, $r = 0.9$ and $P(>r) = 4.4 \times 10^{-6}$. This is the first time, to our knowledge, that a continuum-equivalent width correlation is demonstrated directly in an individual BAL quasar. Some previous evidence was derived as a possible interpretation of the ensemble analysis of BAL variability. In fact, Barlow (1993) found that most variable BALs tend to occur in objects with at least some broadband changes, suggesting some correlation. It is important to notice that, if we exclude the last six epochs, the correlation drops to $r = 0.12$, because during the slow decrease in W_{BAL}, the R continuum stays almost constant, and the correlation is entirely due to the fast increase in W_{BAL} when the R flux decreases significantly.

b) $W_{\mathrm{NAL}r}$ vs. ΔR. At variance with W_{BAL}, the red-NAL equivalent width $W_{\mathrm{NAL}r}$ is only marginally anti-correlated with R, if we consider all the observations. However, this negative correlation becomes more significant if we exclude the last six epochs where there is a significant variation in R.

c) $W_{\mathrm{NAL}b}$ vs. ΔR. The exclusion of the last six epochs corresponds to a negative correlation, but only a marginal one. At variance with *b)*, the points corresponding to the last six epochs lie in the top right of the panel, implying an even weaker correlation when all epochs are considered. This, however, is likely due to the "contamination" of the residual corresponding to the blue NAL, by the absorption of the underlying BAL.

d) $W_{\mathrm{NAL}r}$ vs. $W_{\mathrm{NAL}b}$. A moderate correlation is found, entirely due to the lack of points in the upper right-hand corner. However, if we exclude the last six epochs, the correlation becomes higher and more significant. Again, that the last five epochs do not follow the general trend can be explained by the contamination of $W_{\mathrm{NAL}b}$ due to BAL absorption.

e) $W_{\mathrm{NAL}r}$ vs. W_{BAL}. There is no correlation if we include all the epochs. When excluding the last six epochs, $W_{\mathrm{NAL}r}$ and W_{BAL} show a marginal positive correlation. We stress that this happens even though W_{BAL} is not correlated with R; namely, the correlation of $W_{\mathrm{NAL}r}$ and W_{BAL} is independent of their relation with R. This suggests the possibility that both $W_{\mathrm{NAL}r}$ and W_{BAL} are influenced by the variation in the same ionising continuum (see Hamann et al. 2011).

f) $W_{\mathrm{NAL}b}$ vs. W_{BAL}. The situation is similar to the previous one, except that the points corresponding to the last six epochs lie in the top right-hand corner. This also makes the correlation positive if all the epochs are considered. We notice, however, that this can be explained by the "contamination" of $W_{\mathrm{NAL}b}$ by the BAL absorption, as in *c)*.

We notice that the blue NAL, which roughly covers the interval from -8500 km s^{-1} to -6000 km s^{-1}, lies in the middle of the ejection velocity range of the BAL. This may mean that this NAL is caused by clouds embedded in the BAL outflow, though of course velocity alone is not sufficient to know whether the absorbing clouds are spatially located inside the outflowing BAL gas. Its column density is lower than the column density of the red NAL, as can be seen from the high-resolution Keck spectrum (see Fig. 1). The maxima between the absorption line of the blue NAL reach neither the flux of the emission line nor the continuum, suggesting a contribution from an underlying BAL absorption. The minimal flux is about one tenth of the continuum. On the other hand, the velocities of the red NAL features lie roughly within a 1000 km s^{-1} around the systemic velocity. The minima are saturated and the maxima are close to the pseudo-continuum, implying a covering factor $\xi_1 \approx 1$ for this NAL. Thus the physical conditions of red and blue NALs are different. However, it is difficult to establish whether the differences found in the correlations can be associated to physical differences because of the contamination of the blue NAL caused by the BAL, which would require high-resolution variability studies.

4.3. Structure function analysis

Our unprecedented temporal sampling of the spectral variability of a BAL QSR allows us to apply a structure function (SF) analysis that is commonly adopted in the study of AGN flux variability in the radio (Hughes et al. 1992; Hufnagel & Bregman 1992), optical (Trevese et al. 1994; Vanden Berk et al. 2004; Wilhite et al. 2008; MacLeod et al. 2012), and X-ray bands (Fiore et al. 1998; Vagnetti et al. 2011). In practice, with $N = 28$ observations we can compute $N(N-1)/2 = 378$ values of the unbinned discrete structure function (di Clemente et al. 1996; Trevese et al. 2007):

$$UDSF(\tau_{ij}) = \sqrt{\frac{\pi}{2}} \left| \log[W(t_i)] - \log[W(t_j)] \right|, \tag{6}$$

where W may indicate W_{BAL}, $W_{\mathrm{NAL}r}$, or $W_{\mathrm{NAL}b}$ in turn, t_i and t_j are two observation epochs, and $\tau_{ij} = (t_i - t_j)/(1+z)$ is the rest-frame time delay of the QSO at redshift z. The (binned) structure function can be defined in N_{bin} bins of time delay, centred at τ_k, $k = 1, N_{\mathrm{bin}}$

$$SF(\tau_k) = \frac{1}{M_k} \left[\sum_{i,j} UDSF(\tau_{ij}) \right], \tag{7}$$

where the sum is extended to all the M_k values of UDSF belonging to the kth bin of time delay.

We refer to the logarithm of W for analogy with the studies of flux variability that are commonly analysed in magnitude or logarithm of the flux. It is possible to define an *ensemble* SF by co-adding the UDSFs derived from a sample of objects in each bin. One advantage of this procedure is that it can be applied even with only one pair of observations per object (see e.g. Vanden Berk et al. 2004), provided that there are enough objects in the sample. It should be noted that, thanks to the redshift distribution of the sources, the entire range of rest-frame delays may

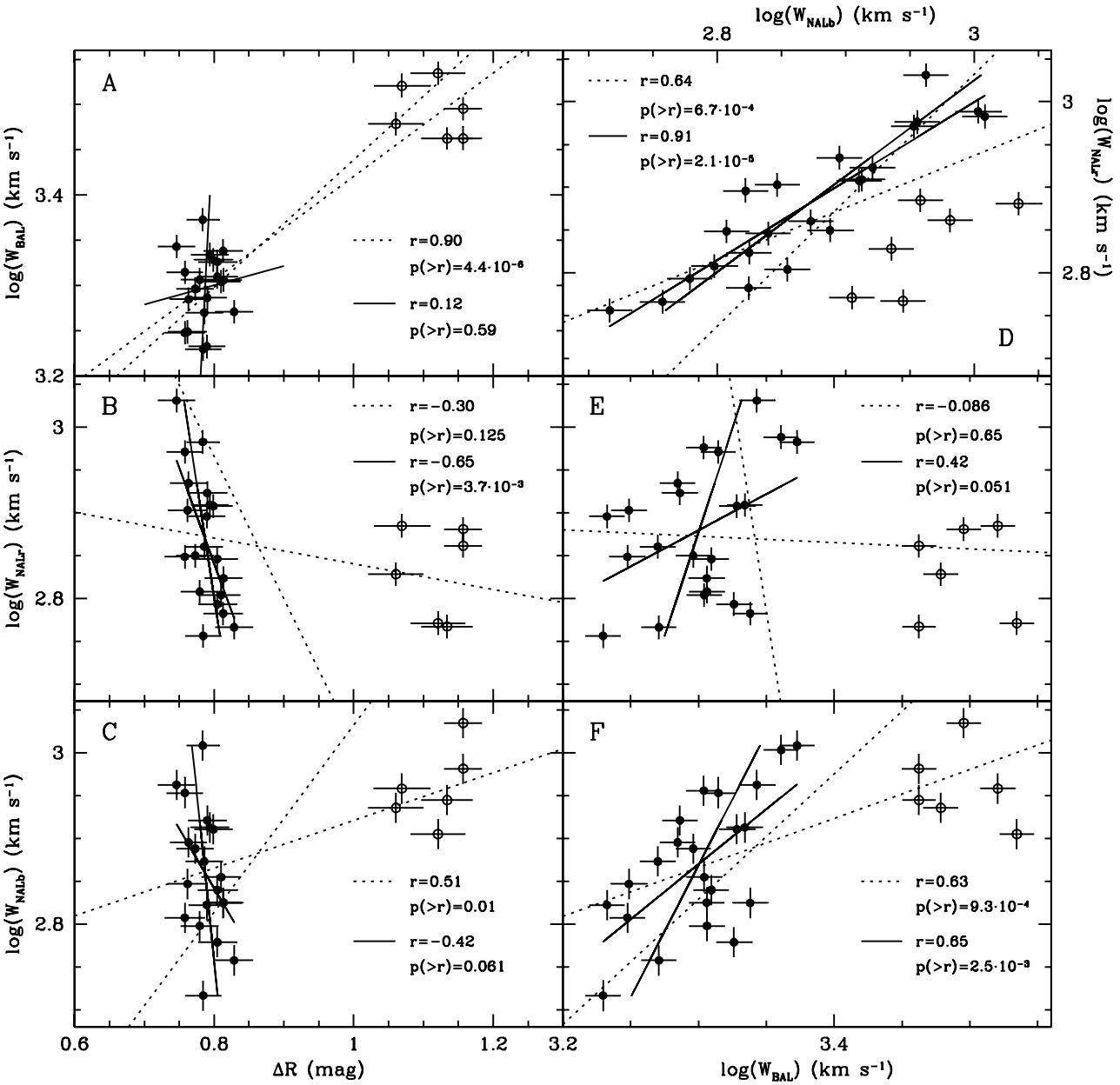

Fig. 7. Six scatter plots for the four quantities $W_{\rm BAL}$, $W_{{\rm NAL}r}$, $W_{{\rm NAL}b}$, and ΔR: *(A)*$W_{\rm BAL}$ vs. ΔR; *(B)*$W_{{\rm NAL}r}$ vs. ΔR; *(C)*$W_{{\rm NAL}b}$ vs. ΔR; *D)*$W_{{\rm NAL}r}$ vs. $W_{{\rm NAL}b}$; *(E)*$W_{{\rm NAL}r}$ vs. $W_{\rm BAL}$; *(F)*$W_{{\rm NAL}b}$ vs. $W_{\rm BAL}$. Filled circles represent data for MJD < 55 000, open circles for MJD > 55 000 (the last 6 epochs). Pairs of regression lines represent linear fits of one variable versus the other and vice versa. Dotted lines refer to the whole set of data, while continuous lines only refer to filled circles. Correlation coefficients and the relevant probabilities are indicated in each panel.

be well sampled. In the top panel of Fig. 8, we show the UDSF for the BAL of APM 08279+5255. For comparison, in the middle panel we show the *ensemble* SF of the BAL equivalent width variability obtained using the data available from the literature (Barlow 1993; Lundgren et al. 2007; Gibson et al. 2008). This corresponds to Fig. 12 of Gibson et al. (2008), in a slightly different presentation.

At first glance it appears that the unbinned distributions of UDSF points in the two panels are similar. The binned SF for the BALs in the two panels also have similar amplitudes and slopes. Thanks to the high redshift of APM 08279+5255, time lags below ten days, down to 0.4 days in the rest frame, are sampled. In the top panel the binned SFs of the red and blue NAL are also reported. They look slightly flatter than the BAL SF owing to larger variability at short time lags, which however could be simply due to a larger noise. In the bottom panel we show the SFs of the two broad absorption components $\rm BAL_1$ and $\rm BAL_2$. It appears that $\rm BAL_1$ varies slightly more than $\rm BAL_2$. This corresponds to about ±20% difference with respect to the total BAL, in the longest delay bin. This is clearly a consequence of the high correlation between the amplitude of the two components, with $W_{{\rm BAL}_2}/W_{{\rm BAL}_1}$ decreasing for increasing $W_{\rm BAL}$, and vice versa (see Fig. 5). Amplitudes and slopes of a power-law fit, $\log SF = A \log \tau + B$, are reported in Table 2.

It is interesting to compare these slope values with typical values found for optical and UV variability, where the slopes are in the range 0.3 to 0.45 (Vanden Berk et al. 2004; Wilhite et al. 2008; Bauer et al. 2009; MacLeod et al. 2012; Welsh et al. 2011). If the absorption variations that we are measuring are in fact due to a change in C^{3+} column density, caused by variations in the

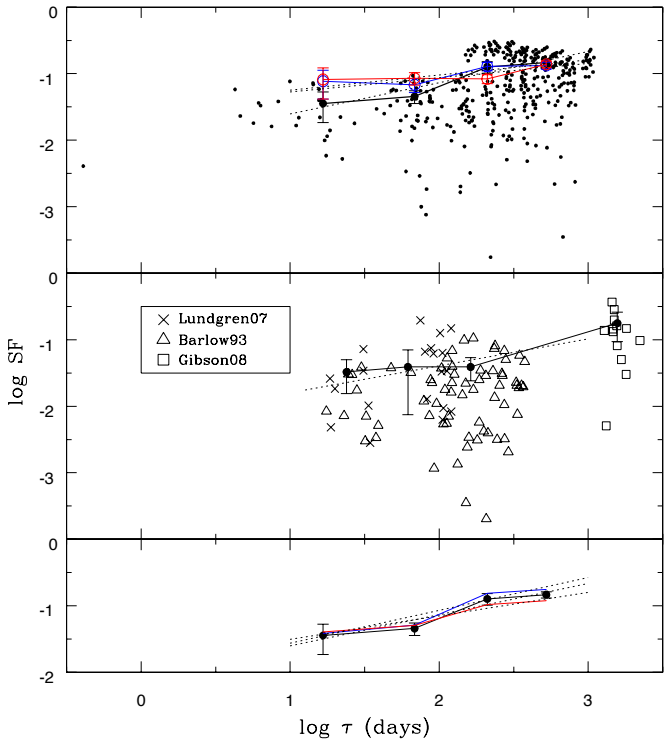

Fig. 8. *Top panel*: structure function of APM 08279+5255; small dots represent the UDSF points (Eq. (6)) relative to BAL variations; filled circles connected with continuous line represent the corresponding binned SF; blue and red open circles connected by continuous lines represent the binned SF for blue and red NALs (blue and red, respectively). The relevant fitting relations corresponding to Table 2 are shown as dotted lines. *Middle panel*: ensemble structure function based on data from the literature (Barlow 1993; Lundgren et al. 2007; Gibson et al. 2008); UDSFs with different symbols as specified in the inset; filled circles connected by continuous line represent the binned ensemble SF and dotted line shows the best fit relation of Table 2. *Bottom panel*: structure functions of the two BAL components of APM 08279+5255; BAL_1 blue line, BAL_2 red line, for comparison black filled circles and the connecting line show the structure function of the total W_{BAL} as in the *top panel.*

Table 2. Best fit parameters of the structure functions.

	A	B
APM 08279 BAL	0.47 ± 0.14	–2.07 ± 0.34
APM 08279 NALb	0.23 ± 0.10	–1.47 ± 0.25
APM 08279 NALr	0.22 ± 0.13	–1.49 ± 0.30
Ensemble BAL	0.41 ± 0.16	–2.20 ± 0.36
APM 08279 BAL_1	0.49 ± 0.15	–2.06 ± 0.37
APM 08279 BAL_2	0.35 ± 0.09	–1.86 ± 0.22

Notes. According to the relation $\log SF = A \log \tau + B$, with τ in days.

ionisation status, we might be observing indirectly the structure function of the 200 Å variability. We notice, for completeness, that we have included in the ensemble structure function analysis only equivalent widths larger than 5 Å on average, as done by Gibson et al. (2008) so that the middle panel of our Fig. 8 is essentially equal to their Fig. 12, except for the change in the variable reported in the ordinates. If instead we include all the points with smaller equivalent width, the SF slope becomes flatter, $A = 0.25$, providing a hint of how the segregation or incompleteness of the data may affect the results. Nonetheless, we can say that, to a first order, the ensemble SF is similar to the SF of APM 08279+5255.

5. Discussion

We can summarise our results as follows.

a) The series of 28 spectroscopic observations spanning a 15-year time base shows that the BAL feature preserves its overall shape, with the two main components varying in a higly correlated way.
b) In spite of this stability, both the BAL and the NAL features exhibit a significant variation in equivalent width.
c) These two results suggest that both density and velocity fields of the absorbing gas remain stable.
d) The R band magnitude shows no systematic trends until MJD ∼ 55 000 but only small oscillations around the mean value; then it increases significantly (∼30% flux decrease) in the last six epochs.
e) The flux decrease in the R band is accompanied by an increase in the BAL absorption. A correlation analysis shows that for MJD < 55 000 there is no correlation between W_{BAL} and R, but the simultaneous and significant increase in W_{BAL} and R after that date determines a statistically significant correlation, $r = 0.9$, $P(>r) = 4.4 \times 10^{-6}$ (panel A in Fig. 7). Some indications of a possible correlation have already been suggested by Barlow (1993), who notice that "most variable BALs tend to occur in objects that show at least some broad-band changes"; however, we stress that it is the first time, to our knowledge, that direct evidence of significant correlation is found.
f) W_{NALb} and W_{NALr} appear correlated, and in particular the correlation and its significance increase considerably ($r = 0.9$, $P(>r) = 2 \times 10^{-5}$) when the last six epochs are excluded. A straightforward interpretation is that the scatter of the points in the last epochs is due to a contamination of the blue NAL by the BAL, while intrinsically the red and blue NALs are strongly correlated. We do not comment further on the correlations of W_{NALb} with the other quantities because disentangling BAL and blue NAL variations would require new high-resolution data.
g) The SF of the BAL variations in APM 08279+5255 has similar slope and amplitude to the ensemble structure function of BAL variations derived from a joint analysis of the data by Barlow (1993), Lundgren et al. (2007), and Gibson et al. (2008), and shown in the middle panel of Fig. 8.
h) The SFs of red and blue NALs of APM 08279+5255 have similar slopes, flatter than for BAL.
i) A comparison of the SFs of the two components of APM 08279+5255 BAL indicates stronger variability of the one with higher ejection velocity.
j) The SF slope of APM 08279+5255 BAL is similar to typical values found for the optical/UV variability of normal QSOs (e.g. MacLeod et al. 2012).

The above results might be easily explained by changes in the ionisation status of the absorbing gas. The different amplitude of W_{BAL_1} and W_{BAL_2} variations, which are strongly correlated, might mean that the two components have different levels of saturation. Under the assumption that absorption variability is driven by changes in the ionising flux ($\lambda \sim 200$ Å), the comparison of W_{BAL} and R changes, before and after MJD ∼ 55 000, would correspond to a change in the average continuum slope between 200 Å and 1500 Å, indicating different physical conditions in the two epochs. This could happen, for instance, if before

MJD $\sim$ 55 000 the ionisation changes come from small variations in the intensity of the ionising source, which can be identified with the inner part of the accretion disk. The continuum at 1500 Å could be substantially unaffected. After MJD $\sim$ 55 000, when a major variation occurs, an absorbing cloud, crossing the line of sight between the ionising continuum source and the gas outflow responsible for the BAL, could reduce both the ionising continuum and the continuum at 1500 Å at the same time, thus causing the observed correlation between $W_{\rm BAL}$ and R.

The sudden increase in $W_{\rm BAL}$ and R after MJD $\sim$ 55 000 does not occur for $W_{{\rm NAL}r}$. Could this different behaviour be due to a delay in NAL variations? At variance with the emission lines, for absorption lines there is no delay caused by the geometry since the absorber lies along the line of sight of continuum photons (Barlow 1993). Nonetheless, the intrinsic delay due to the recombination time of C^{4+} atoms may be significant. Assuming that the different behaviour of $W_{{\rm NAL}r}$ and $W_{\rm BAL}$ is simply because we do not see the $W_{{\rm NAL}r}$ increase yet, we can infer an upper limit on the electron density $n_e \lesssim 1/(\Delta t \alpha_r) \approx 2 \times 10^4$ cm^{-3}, when adopting a minimum (rest-frame) delay $\Delta t \sim 200$ days and $\alpha_r = 2.8 \times 10^{-12}$ cm^3 s^{-1} (Arnaud & Rothenflug 1985). This density is comparable to typical narrow line region densities, thus suggesting this as a possible location of the absorbers. This is also consistent with the covering factor $\xi_1 = 1$ required by the saturation that is observed in the high-resolution Keck spectrum.

Finally we stress that, while ionisation changes can more easily explain correlated variations in different velocity intervals of a BAL structure, in some cases observations show different portions of a BAL varying independently (Hall et al. 2011; Capellupo et al. 2012). The latter are more easily interpreted as due to gas clouds crossing the line of sight. A priori there is no reason to expect that this kind of variation should show the same SF as we observe in our case, where changes in different velocity intervals are strongly correlated. In this sense, the similarity between the SF of APM 08279+5255 and the ensemble SF deduced from the literature, which likely includes cases of BAL variations caused by independent clouds, either provides statistical constraints on geometrical models or implies that changes due to geometrical effects represent a minority of the observed cases.

Acknowledgements. It is a pleasure to acknowledge M. J. Irwin for providing us with the discovery spectrum of APM 08279+5255, D.C. Hines and G.D. Schmidt for the spectrum taken at the Steward Observatory 2.3 m Bok telescope, T. A. Barlow for sending the equivalent width variability data of his Ph.D. Thesis. We are grateful to E. Piconcelli and F. Fiore for useful discussions. We acknowledge S. Benetti and the technical staff of the Asiago Observatory for the support provided during the entire monitoring campaign.

References

Arnaud, M., & Rothenflug, R. 1985, A&AS, 60, 425
Barlow, T. A. 1993, Ph.D. Thesis, California University
Barlow, T. A., Junkkarinen, V. T., Burbidge, E. M., et al. 1992, ApJ, 397, 81
Bauer, A., Baltay, C., Coppi, P., et al. 2009, ApJ, 696, 1241
Blandford, R. D., & McKee, C. F. 1982, ApJ, 255, 419
Capellupo, D. M., Hamann, F., Shields, J. C., Rodríguez Hidalgo, P., & Barlow, T. A. 2011, MNRAS, 413, 908
Capellupo, D. M., Hamann, F., Shields, J. C., Rodríguez Hidalgo, P., & Barlow, T. A. 2012, MNRAS, 422, 3249
Capellupo, D. M., Hamann, F., Shields, J. C., Halpern, J. P., & Barlow, T. A. 2013, MNRAS, 429, 1872
Cattaneo, A., Faber, S. M., Binney, J., et al. 2009, Nature, 460, 213
Chartas, G., Saez, C., Brandt, W. N., Giustini, M., & Garmire, G. P. 2009, ApJ, 706, 644
di Clemente, A., Giallongo, E., Natali, G., Trevese, D., & Vagnetti, F. 1996, ApJ, 463, 466
Downes, D., Neri, R., Wiklind, T., Wilner, D. J., & Shaver, P. A. 1999, ApJ, 513, L1
Egami, E., Neugebauer, G., Soifer, B. T., et al. 2000, ApJ, 535, 561
Ellison, S. L., Lewis, G. F., Pettini, M., et al. 1999, PASP, 111, 946
Ellison, S. L., Ibata, R., Pettini, M., et al. 2004, A&A, 414, 79
Elvis, M. 2000, ApJ, 545, 63
Farrah, D., Lacy, M., Priddey, R., Borys, C., & Afonso, J. 2007, ApJ, 662, L59
Fiore, F., Laor, A., Elvis, M., Nicastro, F., & Giallongo, E. 1998, ApJ, 503, 607
Foltz, C. B., Weymann, R. J., Morris, S. L., & Turnshek, D. A. 1987, ApJ, 317, 450
Gibson, R. R., Brandt, W. N., Schneider, D. P., & Gallagher, S. C. 2008, ApJ, 675, 985
Gibson, R. R., Brandt, W. N., Gallagher, S. C., Hewett, P. C., & Schneider, D. P. 2010, ApJ, 713, 220
Hall, P. B., Anosov, K., White, R. L., et al. 2011, MNRAS, 411, 2653
Hamann, F., Kanekar, N., Prochaska, J. X., et al. 2011, MNRAS, 410, 1957
Hewett, P. C., & Foltz, C. B. 2003, AJ, 125, 1784
Hewett, P. C., Foltz, C. B., & Chaffee, F. H. 1995, AJ, 109, 1498
Hines, D. C., Schmidt, G. D., & Smith, P. S. 1999, ApJ, 514, L91
Hufnagel, B. R., & Bregman, J. N. 1992, ApJ, 386, 473
Hughes, P. A., Aller, H. D., & Aller, M. F. 1992, ApJ, 396, 469
Ibata, R. A., Lewis, G. F., Irwin, M. J., Lehár, J., & Totten, E. J. 1999, AJ, 118, 1922
Irwin, M. J., Ibata, R. A., Lewis, G. F., & Totten, E. J. 1998, ApJ, 505, 529
Ledoux, C., Theodore, B., Petitjean, P., et al. 1998, A&A, 339, L77
Lewis, G. F., Robb, R. M., & Ibata, R. A. 1999, PASP, 111, 1503
Lewis, G. F., Ibata, R. A., Ellison, S. L., et al. 2002, MNRAS, 334, L7
Lundgren, B. F., Wilhite, B. C., Brunner, R. J., et al. 2007, ApJ, 656, 73
Lynds, C. R. 1967, ApJ, 147, 396
MacLeod, C. L., Ivezić, Ž., Sesar, B., et al. 2012, ApJ, 753, 106
Peterson, B. M. 1993, PASP, 105, 247
Proga, D., Stone, J. M., & Kallman, T. R. 2000, ApJ, 543, 686
Srianand, R., & Petitjean, P. 2000, A&A, 357, 414
Tombesi, F., Cappi, M., Reeves, J. N., et al. 2010, A&A, 521, A57
Trevese, D., Kron, R. G., Majewski, S. R., Bershady, M. A., & Koo, D. C. 1994, ApJ, 433, 494
Trevese, D., Paris, D., Stirpe, G. M., Vagnetti, F., & Zitelli, V. 2007, A&A, 470, 491
Turnshek, D. A. 1988, in QSO Absorption Lines: Probing the Universe, eds. J. C. Blades, D. A. Turnshek, & C. A. Norman, 17
Vagnetti, F., Turriziani, S., & Trevese, D. 2011, A&A, 536, A84
Vanden Berk, D. E., Richards, G. T., Bauer, A., et al. 2001, AJ, 122, 549
Vanden Berk, D. E., Wilhite, B. C., Kron, R. G., et al. 2004, ApJ, 601, 692
Welsh, B. Y., Wheatley, J. M., & Neil, J. D. 2011, A&A, 527, A15
Weymann, R., & Foltz, C. 1983, in Liège Int. Astrophysical Colloq., ed. J.-P. Swings, 24, 538
Wilhite, B. C., Brunner, R. J., Grier, C. J., Schneider, D. P., & vanden Berk, D. E. 2008, MNRAS, 383, 1232
York, D. G., Adelman, J., Anderson, Jr., J. E., et al. 2000, AJ, 120, 1579